Quantum enhanced estimation of diffusion

Dominic Branford,[1] Christos N. Gagatsos,[2,1] Jai Grover,[3] Alexander J. Hickey,[3] and Animesh Datta[1]
[1]*Department of Physics, University of Warwick, Coventry, CV4 7AL, United Kingdom*
[2]*College of Optical Sciences, University of Arizona, 1630 E. University Blvd., Tucson, Arizona 85719, USA*
[3]*ESA–Advanced Concepts Team, European Space Research Technology Centre (ESTEC), Keplerlaan 1, Postbus 299, NL-2200AG Noordwijk, The Netherlands*

(Received 14 January 2019; published 30 August 2019)

Momentum diffusion is a possible mechanism for driving macroscopic quantum systems towards classical behavior. Experimental tests of this hypothesis rely on a precise estimation of the strength of this diffusion. We show that quantum-mechanical squeezing offers significant improvements, including when measuring position. For instance, with 10 dB of mechanical squeezing, experiments would require a tenth of proposed free-fall times. Momentum measurement is better by an additional factor of three, while another quadrature is close to optimal. These have particular implications for the space-based MAQRO proposal—where it could rule out the spontaneous collapse theory due to Ghirardi, Rimini, and Weber—as well as terrestrial optomechanical sensing.

DOI: 10.1103/PhysRevA.100.022129

I. INTRODUCTION

Finding a unified description of microscopic and macroscopic systems remains an enduring quest of fundamental physics. One class of proposed solutions are collapse models [1–4] which span continuous spontaneous localization (CSL) [5–7], Karolyhazy [8], Diósi-Penrose [9–12], and quantum gravity [13], as well as collisional decoherence [14]. In the nonrelativistic regime, they posit spatial decoherence due to diffusion in momentum. The outcome is a description of the evolution in terms of a phase-space density distribution obeying a Fokker-Planck diffusion equation [15]. Experimental advances have now made the testing of this proposition a realistic prospect.

Mechanical systems have been used to bound the strength of such diffusive effects. Examples include gravitational-wave detectors [16], the LISA pathfinder experiment [16–18], ultracold cantilevers [19], and trapped ions [20]. Proposals for future experiments which could probe collapse models and further study macroscopic quantum states include the generation of macroscopic superpositions [21–26] and the space-based MAQRO mission [27,28] which formed a key focus of a recent ESA feasibility study [29].

One simple experiment—which forms a part of the MAQRO mission [27,28]—to test collapse models is to let free particles evolve and measure the expanding width of the wave packet. Once all classical noise sources have been ruled out, any excess wave-packet width must be attributed to momentum diffusion associated with collapse models. MAQRO aims to utilize ultracold nanoparticles and exploit the nanogravity of space to observe free fall over 100 s—enabling more precise sensing of momentum diffusion—as represented in Fig. 1.

Quantum techniques such as squeezing allow for more precise estimation [30,31]. Optical squeezing has been identified as valuable to fundamental physics, with squeezing-enhanced interferometry [32] set to enhance laser-interferometric gravitational-wave detectors [33–35] and 15 dB squeezing of optical vacuum reported [36]. It has also found application in photonic-force microscopy [37,38], while microwave squeezing is being used in the search for axion dark matter [39]. Quantum squeezing of mechanical degrees of freedom is beginning to be explored in thermal states [40,41].

In this article, we show that quantum squeezing of the mechanical degree of freedom enables a more precise estimation of the strength of momentum diffusion. This enhancement is attainable with the currently proposed scheme of measuring the position of a particle. We conclude that squeezing can be used to achieve the same precision with reduced free-fall time or center-of-mass cooling. This reduction could be 10-fold for a squeezing of 10 dB. Thus, squeezing can compensate for reduced free-fall times, identified as one of the challenges for MAQRO [27,28] in a recent ESA CDF study [29]. We further show that a momentum measurement is thrice as precise as that of position, while measurement of a more general quadrature is close to optimal. We briefly discuss the potential of the heterodyne and phonon counting measurements.

While our results will be presented in the context of collapse models, observing similar momentum diffusion processes could aid detection of certain dark-matter candidates [42–44]. Since excess heating of wave packets is also a consequence of momentum diffusion [20,45,46], our results imply a quantum enhanced estimation of heating. Finally, the ubiquitous phenomena of Brownian motion is also caused by diffusion. Our results can thus be applied in this very general scenario, as well as in particle tracking used to study biological systems [47,48].

Before presenting our results, we note some recent works that have theoretically considered continuously monitoring a thermal state [49] or squeezing a specific optomechanical coupling [50], with the latter providing no attainable advantage from squeezing when measuring the optical subsystem. Previous works in quantum metrology have analyzed

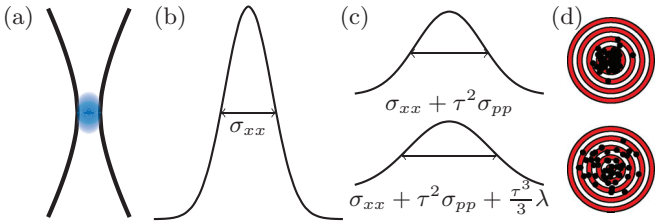

FIG. 1. A pictorial representation of the measurement of wave-packet expansion which forms part of the MAQRO proposals [27,28]. (a) A particle is initially trapped, (b) then released, (c) the free particle wave function expands, more rapidly with a localization term, and (d) the localization rate can be inferred through position measurements. Expansion as depicted in two spatial detections is for illustrative purposes; we analyze only one independent spatial dimension.

quantum-limited estimation of related noise parameters, including loss [51,52], diffusion in phase shifts [53,54] and displacements [55], and classical stochastic processes [56].

II. BACKGROUND

A particle of mass m in a harmonic potential has Hamiltonian $\hat{\mathcal{H}} = \hat{\mathcal{P}}^2/2m + m\omega^2\hat{\mathcal{X}}^2/2$. Dimensionless position and momentum operators are $\hat{x} = \sqrt{m\omega}\hat{\mathcal{X}}/\sqrt{\hbar}$ and $\hat{p} = \hat{\mathcal{P}}/\sqrt{\hbar m\omega}$ whose commutators are given by the matrix $i\Omega$ where

$$\Omega = -i\begin{pmatrix}[\hat{x},\hat{x}] & [\hat{x},\hat{p}]\\ [\hat{p},\hat{x}] & [\hat{p},\hat{p}]\end{pmatrix} = \begin{pmatrix}0 & 1\\ -1 & 0\end{pmatrix}. \tag{1}$$

Quantum states of such a particle have a phase-space representation in terms of the Wigner function of an operator defined as [57, Chap. 1]

$$W_\rho(x,p) = \frac{2}{\pi}\mathrm{Tr}\left[\rho\hat{D}\left(\frac{x+ip}{\sqrt{2}}\right)\hat{\Pi}\hat{D}^\dagger\left(\frac{x+ip}{\sqrt{2}}\right)\right], \tag{2}$$

where $\hat{D}(\alpha) = e^{\alpha\hat{a}^\dagger - \alpha^*\hat{a}}$ and $\hat{\Pi} = e^{i\pi\hat{a}^\dagger\hat{a}}$. Gaussian states are those whose Wigner function is Gaussian and so determined by the averages (displacement vector $\vec{d}$) and covariances (covariance matrix σ) of the position and momentum operators. Examples include thermal, coherent, and squeezed states. A thermal state has covariance matrix $\sigma = \kappa_{\mathrm{th}}\mathbb{1}$, with $\sigma = \mathbb{1}$ corresponding to the ground state.

We focus on the simplest setup to study momentum diffusion, that of a free particle as in Fig. 1. Initially the particle is trapped in a harmonic potential with frequency ω and cooled. Cooling of nanoparticles has been reported to the order of 100 phonons [58,59] with theory anticipating cooling much closer to the ground state [60,61]. After cooling the trapping potential is turned off. The particle then evolves freely under the Hamiltonian $\hat{\mathcal{H}} = \hat{\mathcal{P}}^2/2m$ with Lindblad term $\Lambda[\hat{\mathcal{X}},[\hat{\mathcal{X}},\rho]]$, whose strength Λ is our parameter of interest. The master equation for momentum diffusion for this system—in terms of the dimensionless position and momentum operators—is

$$\frac{\partial\rho}{\partial\tau} = -\frac{i}{2}[\hat{p}^2,\rho] - \frac{1}{4}\lambda[\hat{x},[\hat{x},\rho]], \tag{3}$$

where $\tau = \omega t$ and $\lambda = \Lambda/\Lambda_0$ are dimensionless parameters, and $\Lambda_0 = m\omega^2/(4\hbar)$. Being quadratic the master equation Eq. (3) evolves Gaussian states to Gaussian states [62–64].

TABLE I. Parameter values based on Kaltenbaek *et al.* [28], primarily Table 1 therein.

Localization rate Λ	10^{10}–10^{20} m^{-2} s^{-1}
Free-fall time t	100 s
Mechanical frequency ω	10^5 rad s^{-1}
Mass m	10^8–10^{10} u
Thermal occupation number n_{th}	0.3
Thermal variance ($\kappa_{\mathrm{th}} = 2n_{\mathrm{th}} + 1$)	1.6
Limiting localization[a] ($\Lambda_0 = \frac{m\omega^2}{4\hbar}$)	1.6×10^{26} m^{-2} s^{-1}
Experiment timescale ($\tau = \omega t$)	6.3×10^7

[a]Using $m = 10^8$ u.

Equation (3) can then be transformed to a Fokker-Planck equation [63,65], in this case yielding

$$\frac{\partial}{\partial\tau}W(x,p,\tau) = \left[-p\frac{\partial}{\partial x} + \frac{1}{4}\lambda\frac{\partial^2}{\partial p^2}\right]W(x,p,\tau), \tag{4}$$

which for Gaussian W can be mapped to an equation of motion of form [62,64]

$$\frac{\partial\vec{\mu}}{\partial\tau} = A\vec{\mu}, \quad \frac{\partial\sigma}{\partial\tau} = A\sigma + \sigma A^T + D, \tag{5}$$

where $\vec{\mu}$ and σ are the Gaussian's moments. For an initial Gaussian state with moments $\vec{d}$ and σ the evolved moments under Eq. (4) become

$$\vec{d}(\tau) = \begin{pmatrix}1 & \tau\\ 0 & 1\end{pmatrix}\vec{d}, \tag{6}$$

$$\sigma(\tau) = \begin{pmatrix}1 & \tau\\ 0 & 1\end{pmatrix}\sigma\begin{pmatrix}1 & 0\\ \tau & 1\end{pmatrix} + \lambda\begin{pmatrix}\tau^3/3 & \tau^2/2\\ \tau^2/2 & \tau\end{pmatrix}. \tag{7}$$

To estimate the strength of the momentum diffusion Λ, we begin with a single-mode Gaussian state. Such a state can be described as a thermal state $\kappa_{\mathrm{th}}\mathbb{1}$ with a squeezing $r \geqslant 0$ of the quadrature $\hat{x}\sin\phi + \hat{p}\cos\phi$ giving an initial covariance matrix

$$\sigma = \kappa_{\mathrm{th}}\begin{pmatrix}\cosh 2r + \sinh 2r\cos 2\phi & \sinh 2r\sin 2\phi\\ \sinh 2r\sin 2\phi & \cosh 2r - \sinh 2r\cos 2\phi\end{pmatrix}, \tag{8}$$

with arbitrary displacements. The displacements do not begin with any parameter dependence and do not gain any through the evolution given by Eq. (6), and so their derivative with respect to the parameter satisfies $\partial_\Lambda\vec{d} = 0$. We will consider tuning ϕ to maximize the precision for given thermal variance and squeezing magnitudes, with $\phi = 0$ and $\phi = \pi/2$ corresponding to momentum and position squeezing, respectively.

Our results apply to estimation of diffusion in any scenario governed by Eq. (3) for all values of λ and τ. We will highlight special cases for $\lambda \ll 1$ and $\tau \gg 1$, which is the regime for MAQRO [27,28] as in Table I, and $\kappa_{\mathrm{th}} \sim 1$ which is around the MAQRO regime.

An estimator is required to estimate an unknown parameter from observed data. If limited to statistical noise the precision of the value produced by the estimator can be taken from the variance of that estimator. The Cramér-Rao bound (CRB)

lower bounds the variance of an unbiased estimator as [66–69]

$$(\Delta\widetilde{\Lambda})^2 \geqslant \frac{1}{\nu F(\Lambda)} \geqslant \frac{1}{\nu H(\Lambda)}, \tag{9}$$

where ν is the number of repetitions of an experiment, $\widetilde{\Lambda}$ is an estimator of the parameter Λ, and $F(\Lambda)$ and $H(\Lambda)$ are, respectively, the classical Fisher information (CFI) and quantum Fisher information (QFI). The CFI is a function of the probability distribution [66]

$$F(\Lambda) = \int d\vec{x}\, \frac{1}{P(\Pi_{\vec{x}}|\rho_\Lambda)}\left[\frac{\partial P(\Pi_{\vec{x}}|\rho_\Lambda)}{\partial\Lambda}\right]^2, \tag{10}$$

where the probabilities $P(\Pi_{\vec{x}}|\rho_\Lambda)$ are derived from applying the positive-operator valued measure $\mathbf{\Pi}$ to the state ρ_Λ. The QFI is a function of the state alone [30,31,69]

$$H(\Lambda) = \mathrm{Tr}\big[\rho_\Lambda L_\Lambda^2\big], \tag{11}$$

where L_Λ is the symmetric logarithmic derivative (SLD) defined by $L_\Lambda\rho_\Lambda + \rho_\Lambda L_\Lambda = 2\partial_\Lambda\rho$.

These CFI and QFI provide the CRB and quantum CRB (QCRB), the first and second inequalities of Eq. (9), respectively. The equalities in Eq. (9) are obtained by an optimal measurement, where it exists, and an efficient estimator; we identify such a measurement and the maximum likelihood estimator is asymptotically efficient [66].

For a Gaussian state (where $\partial_\Lambda\vec{d} = 0$) the QFI can be evaluated explicitly as [70,71]

$$H(\Lambda) = \tfrac{1}{2}(\partial_\Lambda\sigma|(\sigma\otimes\sigma - \Omega\otimes\Omega)^{-1}|\partial_\Lambda\sigma), \tag{12}$$

where the inner product is $(A|B) = \mathrm{Tr}[A^T B]$.

III. RESULTS

Using Eqs. (7) and (8), the QCRB can be calculated through Eq. (12) to be

$$(\Delta\widetilde{\Lambda})^2 \geqslant \frac{\Lambda_0^2\big[\big(\kappa_{\rm th}^2 + \tau\kappa_{\rm th}\lambda Z + \frac{\tau^4}{12}\lambda^2\big)^2 - 1\big]}{\frac{\tau^4}{12}\big(1 - \kappa_{\rm th}^2 + \tau\kappa_{\rm th}\lambda Z + \frac{\tau^4}{12}\lambda^2\big) + \frac{\tau^2}{2}\kappa_{\rm th}^2 Z^2}, \tag{13}$$

where $Z = (1 + \tau^2/3)\cosh 2r + [(1 - \tau^2/3)\cos 2\phi + \tau\sin 2\phi]\sinh 2r$. The bound in Eq. (13) behaves as $(\Delta\widetilde{\Lambda})^2 \gtrsim \Lambda^2$ to leading order in Λ.

The QCRB in Eq. (13) is minimized by squeezing or antisqueezing (squeezing the orthogonal quadrature) with squeezing angle (see Appendix A)

$$\phi = \arctan\left(\frac{-3 + \tau^2 - \sqrt{9 + 3\tau^2 + \tau^4}}{3\tau}\right), \tag{14}$$

which tends to 0 for $\tau \gg 1$, corresponding to squeezing of position or momentum. When squeezing at this angle in the regime of $\tau \gg 1$, with $\kappa_{\rm th} = 1$, the QCRB simplifies to

$$(\Delta\widetilde{\Lambda})^2 \gtrsim \Lambda_0^2\frac{8\lambda\big(e^{-2r} + \frac{\tau}{4}\lambda\big)\big(1 + \frac{\tau^3}{6}e^{-2r}\lambda + \frac{\tau^4}{24}\lambda^2\big)}{\frac{2\tau^3}{3}e^{-4r} + \frac{\tau^4}{3}e^{-2r}\lambda + \frac{\tau^5}{12}\lambda^2},$$

with the squeezing r not necessarily positive as antisqueezing may be preferable (see Appendix A).

Measurement of the particle's position is a special case of homodyne detection, which involves measuring a linear combination of the position and momentum quadratures [64,72]. Heterodyne allows for the simultaneous measurement of position and momentum, but with added noise [73,74]. The QCRB can be reached through projection onto eigenstates of the SLD [75], which, for a Gaussian system, entails performing some squeezing and displacement followed by measurement of Fock states [51,64,70]. This additional squeezing is a resource applied to the system after the evolution as part of the measurement and does not improve the precision as an initial squeezing can. Further, in a mechanical system this involves measuring the number of phonons, which remains experimentally demanding [76,77]. In the following, we calculate the performance of all these measurements for estimating Λ.

Homodyne detection at an angle θ measures the quadrature $\hat{q}_\theta = \hat{x}\cos\theta + \hat{p}\sin\theta$. When performed on a Gaussian state the homodyne statistics are Gaussian [72], and the moments are the appropriate marginal of the Wigner function. For a homodyne angle θ the variance of the marginal is

$$\begin{aligned}\Sigma = \kappa_{\rm th}\Bigg(&[(1+\tau^2)\cos^2\theta + \tau\sin 2\theta + \sin^2\theta]\cosh 2r\\ &+\{[(1-\tau^2)\cos^2\theta - \tau\sin 2\theta - \sin^2\theta]\cos 2\phi\\ &+[2\tau\cos^2\theta + \sin 2\theta]\sin 2\phi\}\sinh 2r\\ &+\lambda\left(\frac{\tau^3}{3}\cos^2\theta + \frac{\tau^2}{2}\sin 2\theta + \tau\sin^2\theta\right)\Bigg),\end{aligned} \tag{15}$$

and as the Wigner function's mean is parameter-independent, so is the marginal's. The choices $\theta = 0$ and $\theta = \pi/2$ correspond to measurement of position and momentum, respectively. We will consider the optimization of θ, which more generally requires measuring a linear combination of the position and momentum operators.

For a Gaussian probability distribution with a parameter-independent mean, the CFI is [66, Chap. 3]

$$F(\Lambda) = \tfrac{1}{2}\mathrm{Tr}\big[\Sigma^{-1}\partial_\Lambda\Sigma\Sigma^{-1}\partial_\Lambda\Sigma\big], \tag{16}$$

where Σ is the variance of the Gaussian distribution. Using Eqs. (15) and (16), the CRB for homodyne along an angle θ is

$$\begin{aligned}(\Delta\widetilde{\Lambda})^2 \geqslant 2\Lambda_0^2\Bigg[\lambda + \kappa_{\rm th}\Bigg(&\frac{\tau^2\cos^2\theta + \tau\sin 2\theta + 1}{\frac{\tau^3}{3}\cos^2\theta + \frac{\tau^2}{2}\sin 2\theta + \tau\sin^2\theta}\cosh 2r\\ &-\frac{(\tau^2\cos^2\theta + \tau\sin 2\theta - \cos 2\theta)\cos 2\phi - \big(2\tau\cos^2\theta + \sin 2\theta\big)\sin 2\phi}{\frac{\tau^3}{3}\cos^2\theta + \frac{\tau^2}{2}\sin 2\theta + \tau\sin^2\theta}\sinh 2r\Bigg)\Bigg]^2.\end{aligned} \tag{17}$$

To leading order in Λ this is $(\Delta\widetilde{\Lambda})^2 \gtrsim 2\Lambda^2$, which occurs when the first term in the square dominates, whereas when that can be neglected the bound is a Λ-independent constant. The bound on estimating the diffusion Λ from position ($\theta = 0$) measurement is

$$(\Delta\widetilde{\Lambda})^2 \geqslant 2\Lambda_0^2\left[\lambda + \kappa_{\rm th}\left(\frac{[1+\tau^2]\cosh 2r + \{[1-\tau^2]\cos 2\phi + 2\tau\sin 2\phi\}\sinh 2r}{\tau^3/3}\right)\right]^2, \tag{18}$$

which behaves as

$$(\Delta\widetilde{\Lambda})^2 \gtrsim 2\Lambda_0^2\left[\lambda + \kappa_{\rm th}\frac{\cosh 2r - \sinh 2r\cos 2\phi}{\tau/3}\right]^2, \tag{19}$$

for $\tau \gg 1$. Instead, for measuring the momentum ($\theta = \pi/2$) the bound on estimating the diffusion Λ is

$$(\Delta\widetilde{\Lambda})^2 \geqslant 2\Lambda_0^2\left[\lambda + \kappa_{\rm th}\frac{\cosh 2r - \sinh 2r\cos 2\phi}{\tau}\right]^2, \tag{20}$$

which (neglecting squeezing) matches the large τ limit of position measurements when $\lambda \gg \kappa_{\rm th}/\tau$ and is a factor of 9 better when $\lambda \ll \kappa_{\rm th}/\tau$.

The optimal input squeezing angle ϕ can in general be found by minimizing the coefficient of $\sinh 2r$ in Eq. (17), which gives

$$\phi = -\arctan\left(\frac{1}{\tau + \tan\theta}\right). \tag{21}$$

For momentum measurements ($\theta = \pi/2$) this squeezing angle is $\phi = 0$ (squeezing of momentum), whereas for position measurements ($\theta = 0$) this is $\phi = -\arctan(1/\tau)$ tending to $\phi = -\pi/2$ for $\tau \ll 1$, and $\phi = 0$ for $\tau \gg 1$.

In general the squeezing angle in Eq. (21) produces a precision

$$(\Delta\widetilde{\Lambda})^2 \geqslant 2\Lambda_0^2[\lambda + \kappa_{\rm th}e^{-2r}\chi(\tau,\theta)]^2, \tag{22}$$

from which the unsqueezed case ($r = 0$) can also be extracted, where

$$\chi(\tau,\theta) = \frac{\tau^2\cos^2\theta + \tau\sin 2\theta + 1}{\frac{\tau^3}{3}\cos^2\theta + \frac{\tau^2}{2}\sin 2\theta + \tau\sin^2\theta}. \tag{23}$$

One effect of squeezing is equivalent to an effective reduction of $\kappa_{\rm th}$ by e^{-2r}. Unlike reducing the center-of-mass motion—which reaches $\kappa_{\rm th} = 1$ at absolute zero—this squeezing allows an unlimited reduction in the second term. For $\tau \gg 1$ (as $\chi \sim 1/\tau$) the same squeezing could instead be considered as an effective increase in τ by a factor of e^{2r} to obtain the same precision from a much shorter free-fall time.

When the quadrature given by Eq. (21) is squeezed, the homodyne angle which minimizes the bound in Eq. (22) is

$$\theta = -\arctan\left(\frac{3 + 2\tau^2 + \sqrt{9 + 3\tau^2 + \tau^4}}{3\tau}\right), \tag{24}$$

which tends to $\theta \approx -\pi/2 + 1/\tau$ for $\tau \gg 1$. Measuring the quadrature given by Eq. (24) with squeezing as Eq. (21) gives a precision

$$(\Delta\widetilde{\Lambda})^2 \geqslant 2\Lambda_0^2\left[\lambda + \kappa_{\rm th}e^{-2r}\frac{3 + \tau^2 - \sqrt{9 + 3\tau^2 + \tau^4}}{\tau^3/2}\right]^2. \tag{25}$$

Performing homodyne on the quadrature of Eq. (24) does not in general attain the QCRB. When λ dominates, the QCRB behaves as Λ^2 while any homodyne terms tend to $2\Lambda^2$. In the $\tau \gg 1$ regime, one could improve on the precision by no more than a factor of 2 using heterodyne detection (see Appendix B). Figure 6 suggests that heterodyne otherwise shows little promise.

Phonon counting—in combination with displacement and squeezing operations—can in principle attain the QCRB for all λ and τ as the SLD is a quadratic operator in the quadrature operators [64,70] and so has eigenstates which are squeezed-displaced Fock states. The additional squeezing required to attain the QCRB is derived in full generality in Appendix C. For MAQRO, this squeezing seems nugatory, with 79 dB required to attain the QCRB for $\Lambda = 10^{20}\ \mathrm{m^{-2}\,s^{-1}}$, which would improve precision only by a factor of $\sqrt{2}$, to 158 dB for $\Lambda = 10^{10}\ \mathrm{m^{-2}\,s^{-1}}$, where the improvement on position measurements would be more pronounced. In other scenarios, however, this could be worthwhile. For $\tau \ll 1$ and $\lambda\tau^2 \lesssim 1$ the squeezing needed is only $e^{2z} \approx 1 + \tau \approx 1$, while for $\tau \gg 1$ and $\lambda\tau \gtrsim 1$ this goes to $e^{2z} \approx 2\tau/\sqrt{3}$.

IV. DISCUSSION

Figure 2 shows the potential improvement in precision for estimating diffusion via momentum or general quadrature measurements, or through squeezing, for MAQRO parameters

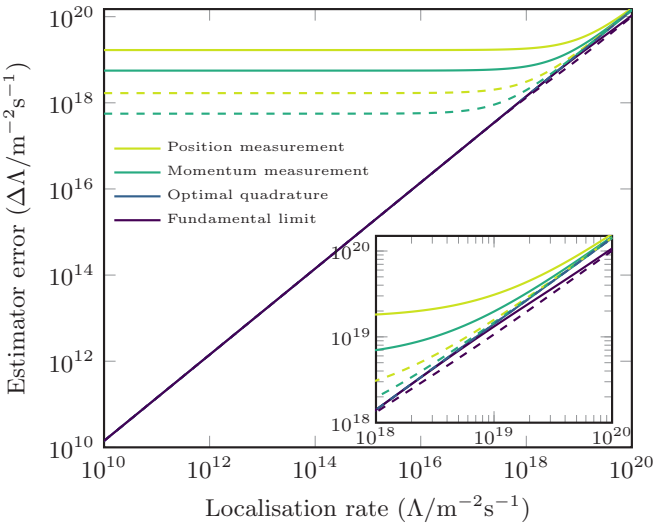

FIG. 2. Precision of estimating momentum diffusion from wave-packet expansion for MAQRO parameters (Table I). Dashed lines denote a squeezing of 10 dB. The optimal homodyne and fundamental limit lines overlap until around $\Lambda \sim 10^{20}\ \mathrm{m^{-2}\,s^{-1}}$. Three years' data collection with $t = 100$ s yields $\nu \sim 10^6$ repetitions.

as given in Table I. For reference, position measurement is the present proposal. We propose squeezing of the momentum quadrature, which offers a substantial improvement across much of the pertinent Λ range for both measurement of position and momentum, with 10 dB enabling an order of magnitude higher resolution of Λ. Measuring the quadrature described by Eq. (24) allows further improvement, keeping within a factor of two of the QCRB across the whole regime.

Our bounds can be mapped to the wealth of diffusive processes whose parameters enter into the observed diffusion rate Λ. In the case of (mass-proportional) CSL the two parameters of interest are λ^{CSL} and r_{C}, the time and length scales in the model. The observed diffusion rate Λ for a free sphere of mass m and radius r_{s} is—as a function of λ^{CSL} and r_{C}—given by [28,45]

$$\Lambda = \frac{\lambda^{\mathrm{CSL}}}{4r_{\mathrm{C}}^2}\left(\frac{m}{m_0}\right)^2 f\left(\frac{r_{\mathrm{s}}}{r_{\mathrm{C}}}\right), \tag{26}$$

where m_0 is a reference (nucleon) mass and $f(x) = \frac{6}{x^4}[1 - \frac{2}{x^2} + (1 + \frac{2}{x^2})e^{-x^2}]$. From this bounds on λ^{CSL} as a function of r_{C} can be calculated using

$$\Delta\lambda^{\mathrm{CSL}} = 4r_{\mathrm{C}}^2\left[\left(\frac{m}{m_0}\right)^2 f\left(\frac{r_{\mathrm{s}}}{r_{\mathrm{C}}}\right)\right]^{-1}\Delta\Lambda. \tag{27}$$

To describe the minimal discernible λ^{CSL} for measurement of a mechanical quadrature we take the limit of the single-shot CRB $\lambda_0^{\mathrm{CSL}} = \lim_{\lambda^{\mathrm{CSL}}\to 0}\Delta\lambda^{\mathrm{CSL}}$. Allowing for ν independent repetitions the uncertainty can be reduced to $\Delta\lambda^{\mathrm{CSL}} \approx \sqrt{\frac{1}{\nu}}\left(\sqrt{\frac{1}{\nu}}+1\right)\lambda_0^{\mathrm{CSL}}$ at $\lambda^{\mathrm{CSL}} \approx \lambda_0^{\mathrm{CSL}}/\sqrt{\nu}$. To ensure any deviation can be recognized with statistical significance we take the minimum detectable collapse rate $\lambda_{\mathrm{min}}^{\mathrm{CSL}}$ to be $\lambda_{\mathrm{min}}^{\mathrm{CSL}} \sim \frac{2}{\sqrt{\nu}}\lambda_0^{\mathrm{CSL}}$. Thus, for a quadrature measurement we take the minimum resolvable λ^{CSL} to be given by $\lambda_{\mathrm{min}}^{\mathrm{CSL}} = \frac{2}{\sqrt{\nu}}\lim_{\lambda^{\mathrm{CSL}}\to 0}\Delta\lambda^{\mathrm{CSL}}$ in Eq. (17).

For MAQRO such bounds can be seen in Fig. 3 for the position, momentum, and optimal quadratures. For position or momentum measurements with up to 10 dB squeezing the bounds are competitive across 10^{-8}–10^{-5} m; below 10^{-8} m x-ray emission data begin to provide a tighter bound [78], while above 10^{-5} m LISA Pathfinder data are tighter [16,18]. Additional squeezing can of course further reduce the uncertainty, with 20 dB of squeezing sufficient to match the theoretical minimum collapse rate to above 10^{-7} m. This would include testing the original parameters suggested by Ghirardi *et al.* [15].

The optimal quadrature identified in Eq. (24) meanwhile could yield a conclusive test of the conventional CSL model at a precision of six orders of magnitude more than the theoretical lower bound on CSL [7]. Attaining the QCRB can offer further improvements; however, this would be of little value to MAQRO if the optimal homodyne sensitivity can be reached.

In conclusion, we have shown that squeezing could be used to compensate for reduced free-fall times, an aspect which a recent ESA CDF study [29] has identified as one of the more demanding of the original proposals [27,28]. As, for both Eq. (19) and Eq. (20), the precision is constant for $e^{2r}\tau$ being constant, longer effective free-fall times can be generated through mechanical squeezing. We have also shown the efficacy of momentum and general quadrature measurements over the proposed position measurement.

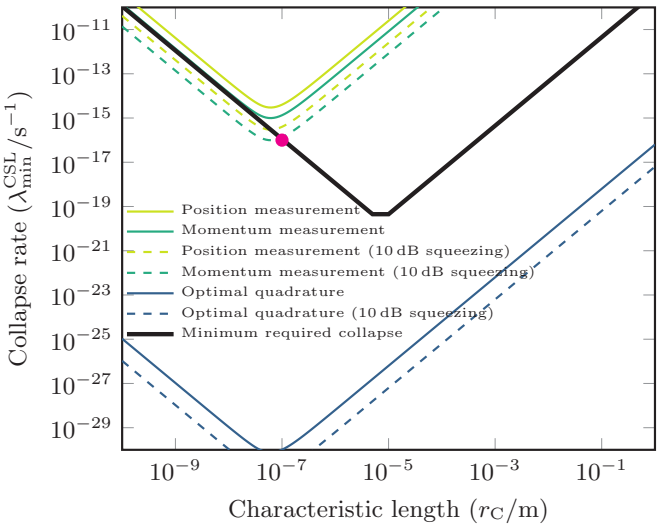

FIG. 3. Minimum detectable collapse rate for three years of observation with a 100 nm radius sphere of mass 5.5×10^9 u, with other parameters as Table I. The minimum required collapse rate given is based on the criteria of Ref. [7] to ensure macroscopic objects rapidly collapse to classical states. The magenta dot represents the values originally proposed by Ghirardi *et al.* [15].

ACKNOWLEDGMENTS

We thank Rainer Kaltenbaek, Hendrik Ulbricht, Matteo Carlesso, and Francesco Albarelli for illuminating discussions. This study has been supported by the European Space Agency's Ariadna scheme (Study Ref. 17-1201a), the U.K. EPSRC (EP/K04057X/2), and the U.K. National Quantum Technologies Programme (EP/M01326X/1, EP/M013243/1). D.B. has received support for travel and attendance at workshops from COST Action QTSpace (CA15220).

APPENDIXES

Appendix A calculates the necessary squeezing angle to maximize precision for the fundamental limit and quadrature measurements. Appendix B calculates the CRB of heterodyne measurements. Appendix C derives the necessary squeezing required to then project onto the eigenstates of the SLD by phonon counting. Appendix D compares performance of the fundamental limit, optimal homodyne quadrature, and heterodyne measurements. Appendix E translates the bounds on the observed diffusion rate Λ to the parameters of CSL.

APPENDIX A: OPTIMAL SQUEEZING

1. Fundamental limit

The QCRB is

$$(\Delta\Lambda)^2 \geqslant B = \Lambda_0^2 \frac{\left(\kappa_{\rm th}^2 + \tau\kappa_{\rm th}\lambda Z + \frac{\tau^4}{12}\lambda^2\right)^2 - 1}{\frac{\tau^4}{12}\left(\kappa_{\rm th}^2 + \tau\kappa_{\rm th}\lambda Z + \frac{\tau^4}{12}\lambda^2\right) + \frac{\tau^4}{12}\left(1 - 2\kappa_{\rm th}^2\right) + \frac{1}{2}\kappa_{\rm th}^2\tau^2 Z^2}, \tag{A1}$$

where

$$Z = \left(1 + \frac{\tau^2}{3}\right)\cosh 2r + \left[\left(1 - \frac{\tau^2}{3}\right)\cos 2\phi + \tau \sin 2\phi\right]\sinh 2r. \tag{A2}$$

Minima with respect to the squeezing angle of the bound in Eq. (A1) are either solutions of $\frac{\partial B}{\partial Z} = 0$ or $\frac{\partial Z}{\partial \phi} = 0$ as

$$\frac{\partial B}{\partial \phi} = \frac{\partial B}{\partial Z}\frac{\partial Z}{\partial \phi}, \tag{A3}$$

and the second derivative

$$\frac{\partial^2 B}{\partial \phi^2} = \frac{\partial^2 B}{\partial Z^2}\left(\frac{\partial Z}{\partial \phi}\right)^2 + \frac{\partial B}{\partial Z}\frac{\partial^2 Z}{\partial \phi^2}, \tag{A4}$$

distinguishes minima and maxima. The stationary points of $B(Z)$ are

$$Z_\pm = \frac{144\left(1 - \kappa_{\rm th}^4\right) + 24\lambda^2\tau^4\left(1 - 2\kappa_{\rm th}^2\right) + \lambda^4\tau^8 \pm \left|12\left(1 - \kappa_{\rm th}^2\right) + \lambda^2\tau^4\right|\sqrt{\left[12\left(1 + \kappa_{\rm th}^2\right) + \lambda^2\tau^4\right]^2 - 48\lambda^2\kappa_{\rm th}^2\tau^4}}{288\lambda\kappa_{\rm th}^3\tau}, \tag{A5}$$

where the negative root is not possible with $r > 0$ and for the positive root $\frac{\partial^2 B}{\partial Z^2} < 0$, and this means that the minimum of B is found for $\frac{\partial Z}{\partial \phi} = 0$. The stationary points of $Z(\phi)$ are

$$\phi_\pm = \arctan\left(\frac{-3 + \tau^2 \pm \sqrt{9 + 3\tau^2 + \tau^4}}{3\tau}\right), \tag{A6}$$

where we have

$$(\phi_+ - \phi_-) \mod \pi = \frac{\pi}{2} \tag{A7}$$

as $\tan(\phi_+)\tan(\phi_-) = -1$. Hence we recognize that squeezing the quadrature $\hat{x}_{\phi_+}$ is equivalent to antisqueezing of the orthogonal quadrature $\hat{x}_{\phi_-} = \hat{x}_{\phi_+ + \frac{\pi}{2}}$. This follows as $r > 0$ and $\phi \in [0, \pi]$, and $r \in \mathbb{R}$ and $\phi \in [0, \pi/2]$ are equivalent parametrizations of the same squeezings; squeezing a quadrature $\hat{x}_\phi$ is equivalent to antisqueezing the quadrature $\hat{x}_{\phi+\pi/2}$.

As $B(Z_+)$ is a maximum and $Z_- < 0$ is outside the range of $Z(\phi)$ at least one of $\phi_\pm$ is a minimum of $B(\phi)$. We therefore find the global minimum of $B(\phi)$ by finding the smaller of $B(\phi_+)$ and $B(\phi_-)$. For $Z(\phi_\pm)$,

$$Z(\phi_\pm) = \left[\left(1 + \frac{\tau^2}{3}\right)\cosh 2r \pm \frac{\sqrt{9 + 3\tau^2 + \tau^4}}{3}\sinh 2r\right], \tag{A8}$$

where we note that exchanging $\phi_+ \to \phi_-$ is equivalent to $r \to -r$.

For these squeezing angles ($\phi_\pm$) the bound [Eq. (A1)] is

$$\begin{aligned}(\Delta\Lambda)^2 \geqslant \Lambda_0^2 \Bigg(&\left\{\kappa_{\rm th}^2 + \tau\kappa_{\rm th}\lambda\left[\left(1 + \frac{\tau^2}{3}\right)\cosh 2r \pm \frac{\sqrt{9 + 3\tau^2 + \tau^4}}{3}\sinh 2r\right] + \frac{\tau^4}{12}\lambda^2\right\}^2 - 1\Bigg) \\ &\times \Bigg(\frac{\tau^4}{12}\left\{\kappa_{\rm th}^2 + \tau\kappa_{\rm th}\lambda\left[\left(1 + \frac{\tau^2}{3}\right)\cosh 2r \pm \frac{\sqrt{9 + 3\tau^2 + \tau^4}}{3}\sinh 2r\right] + \frac{\tau^4}{12}\lambda^2\right\} \\ &+ \frac{\tau^4}{12}\left(1 - 2\kappa_{\rm th}^2\right) + \frac{\tau^2}{2}\kappa_{\rm th}^2\left[\left(1 + \frac{\tau^2}{3}\right)\cosh 2r \pm \frac{\sqrt{9 + 3\tau^2 + \tau^4}}{3}\sinh 2r\right]^2\Bigg)^{-1},\end{aligned} \tag{A9}$$

which can be written as

$$\frac{(a \pm b)^2 - 1}{c \pm d}, \tag{A10}$$

where

$$a = \kappa_{\rm th}^2 + \kappa_{\rm th}\lambda\tau\left(1 + \frac{\tau^2}{3}\right)\cosh 2r + \frac{\tau^4}{12}\lambda^2, \tag{A11}$$

$$b = \kappa_{\rm th}\lambda\tau\,\frac{\sqrt{9 + 3\tau^2 + \tau^4}}{3}\sinh 2r, \tag{A12}$$

$$c = \frac{\tau^4}{12}\left[1 - \kappa_{\rm th}^2 + \kappa_{\rm th}\lambda\tau\left(1 + \frac{\tau^2}{3}\right)\cosh 2r + \frac{\tau^4}{12}\lambda^2\right] + \frac{\tau^2}{2}\kappa_{\rm th}^2\left[\left(1 + \frac{\tau^2}{3}\right)^2\cosh^2 2r + \left(1 + \frac{\tau^2}{3} + \frac{\tau^4}{9}\right)\sinh^2 2r\right], \tag{A13}$$

$$d = \kappa_{\rm th}\lambda\frac{\tau^5}{12}\frac{\sqrt{9 + 3\tau^2 + \tau^4}}{3}\sinh 2r + \kappa_{\rm th}^2\tau^2\left(1 + \frac{\tau^2}{3}\right)\frac{\sqrt{9 + 3\tau^2 + \tau^4}}{3}\cosh 2r\sinh 2r, \tag{A14}$$

where we have a, b, c, and d all positive as well as $a > b + 1$ and $c > d$. The squeezing angle ϕ_+ therefore offers a better precision for

$$c < d\left(\frac{a^2 + b^2 - 1}{2ab}\right), \tag{A15}$$

which in this case is

$$\begin{aligned} 0 > \lambda\tau\Bigg[&-\kappa_{\rm th}^4\left(1 + 3\frac{\tau^2}{4} + \frac{\tau^4}{9}\right) + \frac{\tau^2}{12}\left(1 + \frac{\lambda^2\tau^4}{12}\right)^2 + \kappa_{\rm th}^2\frac{\tau^2}{6}\left(1 - \frac{\lambda^2\tau^4}{12}\right)\Bigg] \\ &+ \kappa_{\rm th}\left(1 + \frac{\tau^2}{3}\right)\left[1 - \kappa_{\rm th}^4 + \frac{\lambda^2\tau^4}{6}(1 - 2\kappa_{\rm th}^2) + \left(\frac{\lambda^2\tau^4}{12}\right)^2\right]\cosh 2r - \frac{\tau^3}{6}\kappa_{\rm th}^4\lambda\cosh 4r. \end{aligned} \tag{A16}$$

2. Homodyne detection

The CRB for homodyne measurement of the quadrature $\hat{x}\cos\theta + \hat{p}\sin\theta$ is

$$\begin{aligned} (\Delta\Lambda)^2 \geqslant 2\Lambda_0^2\Bigg[\lambda + \kappa_{\rm th}\Bigg(&\frac{[1 + \tau^2]\cos^2\theta + \tau\sin 2\theta + \sin^2\theta}{\frac{1}{3}\tau^3\cos^2\theta + \frac{1}{2}\tau^2\sin 2\theta + \tau\sin^2\theta}\cosh 2r \\ &+ \frac{\{[1 - \tau^2]\cos^2\theta - \tau\sin 2\theta - \sin^2\theta\}\cos 2\phi + \{2\tau\cos^2\theta + \sin 2\theta\}\sin 2\phi}{\frac{1}{3}\tau^3\cos^2\theta + \frac{1}{2}\tau^2\sin 2\theta + \tau\sin^2\theta}\sinh 2r\Bigg)\Bigg]^2. \end{aligned} \tag{A17}$$

a. Optimal squeezing

The bound is minimized with respect to the squeezing angle ϕ by minimizing the coefficient of $\sinh 2r$,

$$[(1 - \tau^2)\cos^2\theta - \tau\sin 2\theta - \sin^2\theta]\cos 2\phi + [2\tau\cos^2\theta + \sin 2\theta]\sin 2\phi, \tag{A18}$$

which has minima

$$\phi = -\arctan\left(\frac{1}{\tau + \tan\theta}\right), \tag{A19}$$

for which squeezing angle the CRB becomes

$$(\Delta\Lambda)^2 \geqslant 2\Lambda_0^2\left[\lambda + e^{-2r}\kappa_{\rm th}\left(\frac{[1 + \tau^2]\cos^2\theta + \tau\sin 2\theta + \sin^2\theta}{\frac{1}{3}\tau^3\cos^2\theta + \frac{1}{2}\tau^2\sin 2\theta + \tau\sin^2\theta}\right)\right]^2. \tag{A20}$$

The optimal homodyne detection can then be recognized as the angle θ

$$\theta = -\arctan\left(\frac{3 + 2\tau^2 + \sqrt{9 + 3\tau^2 + \tau^4}}{3\tau}\right), \tag{A21}$$

and when this homodyne angle is used the optimal squeezing angle is

$$\varphi = \arctan\left(\frac{3\tau}{3 - \tau^2 + \sqrt{9 + 3\tau^2 + \tau^4}}\right). \tag{A22}$$

b. Position and momentum squeezing

Squeezing of position and momentum can be evaluated with $\phi = 0$, with $r > 0$ corresponding to squeezing of momentum while $r < 0$ is a squeezing $|r|$ of position. For $\phi = 0$ the CRB [Eq. (A17)] becomes

$$(\Delta\Lambda)^2 \geqslant 2\Lambda_0^2\left[\lambda + \kappa_{\rm th}\left(\frac{e^{2r}\cos^2\theta + e^{-2r}(\tau^2\cos^2\theta + \tau\sin 2\theta + \sin^2\theta)}{\frac{1}{3}\tau^3\cos^2\theta + \frac{1}{2}\tau^2\sin 2\theta + \tau\sin^2\theta}\right)\right]^2. \tag{A23}$$

The optimal homodyne quadrature is then

$$\theta = -\arctan\left(\frac{3e^{4r} + 2\tau^2 + \sqrt{9e^{8r} + 3e^{4r}\tau^2 + \tau^4}}{3\tau}\right), \tag{A24}$$

which gives a precision

$$(\Delta\Lambda)^2 \geqslant 2\Lambda_0^2\left[\lambda + \kappa_{\rm th}\left(\frac{2(3e^{2r} + e^{-2r}\tau^2 - \sqrt{9e^{4r} + 3\tau^2 + e^{-4r}\tau^4})}{\tau^3}\right)\right], \tag{A25}$$

where squeezing of position ($r < 0$) is beneficial for $\tau < \sqrt{3}$ while squeezing of momentum (antisqueezing of position, $r > 0$) is beneficial for $\tau > \sqrt{3}$.

APPENDIX B: HETERODYNE DETECTION

Heterodyne detection is the projection onto the overcomplete basis of Gaussian states, which amounts to sampling from the Husimi Q function [73,74]. The Q function can be extracted from the Wigner function as [57]

$$Q(x, p) = \frac{1}{\pi}\int dx'dp'W(x', p')\exp[-(x - x')^2 - (p - p')^2], \tag{B1}$$

which is a convolution, and so for a Gaussian Wigner function with moments $\vec{d}$ and σ the Q function will be Gaussian with moments $\vec{d}$ and $\sigma + \mathbb{1}$ [64, Chap. 5].

The mean of the distribution again contains no parameter dependence, and so Eq. (16) can also be applied here. The covariances from heterodyne detection are

$$\Sigma(\tau) = \begin{pmatrix} 1 + \Sigma_{xx} + 2\tau\Sigma_{xp} + \tau^2\Sigma_{pp} + \frac{1}{3}\lambda\tau^3 & \Sigma_{xp} + \tau\Sigma_{pp} + \frac{1}{2}\lambda\tau^2 \\ \Sigma_{xp} + \tau\Sigma_{pp} + \frac{1}{2}\lambda\tau^2 & 1 + \Sigma_{pp} + \lambda\tau \end{pmatrix}, \tag{B2}$$

giving a CRB of

$$(\Delta\Lambda)^2 \geqslant \frac{12\Lambda_0^2|\Sigma(\tau)|^2}{\tau^4|\Sigma(\tau)| + 6\tau^2\left(1 + \Sigma_{xx} + \tau\Sigma_{xp} + \frac{\tau^2}{3}\Sigma_{pp}\right)^2 + 2\tau^4\left[1 + \Sigma_{xx} - \Sigma_{pp} - \Sigma_{xx}\Sigma_{pp} + \Sigma_{xp}^2 + \frac{\tau^2}{3}(1 - \Sigma_{pp})\right]}, \tag{B3}$$

where $|\Sigma|$ is the determinant, and Σ_{xx}, Σ_{xp}, and Σ_{pp} are the initial variances and covariance of the position and momentum operators. Without mechanical squeezing ($r = 0$) this is

$$(\Delta\Lambda)^2 \geqslant \frac{6\Lambda_0^2\left[(1 + \kappa_{\rm th})^2 + \kappa_{\rm th}\tau^2 + \lambda(1 + \kappa_{\rm th})\tau\left(1 + \frac{\tau^2}{3}\right) + \frac{\tau^4}{12}\lambda^2\right]^2}{\frac{\tau^2}{3}\left[\left(1 + \kappa_{\rm th}^2\right)(9 + 3\tau^2 + \tau^4) + \kappa_{\rm th}(18 + 6\tau^2 - \tau^4)\right] + \frac{\tau^4}{2}\left[(1 + \kappa_{\rm th})^2 + \kappa_{\rm th}\tau^2 + \lambda(1 + \kappa_{\rm th})\tau\left(1 + \frac{\tau^2}{3}\right) + \frac{\tau^4}{12}\lambda^2\right]}. \tag{B4}$$

APPENDIX C: OPTIMAL MEASUREMENT

For a Gaussian system the SLD is a Hermitian operator, quadratic in the quadrature operators [64,70]. Any such Hermitian operator, quadratic in the quadrature operators, can be transformed through some squeezing and displacement to an operator diagonal in the Fock basis [64,70].

The SLD is primarily defined through identification of $L^{(2)}$, which is given by [64,70]

$$\sigma L^{(2)}\sigma + \Omega L^{(2)}\Omega = \partial\sigma, \tag{C1}$$

which for a state with constant zero displacements $\vec{d} = 0$ then gives the SLD [64,70]

$$L_{\rho_\Lambda} = (\hat{x} \quad \hat{p}) L^{(2)} \begin{pmatrix} \hat{x} \\ \hat{p} \end{pmatrix} - \frac{1}{2}\mathrm{Tr}[L^{(2)}\sigma]. \tag{C2}$$

The covariance matrix which we wish to solve for Eq. (C1) is Eq. (7), which gives $L^{(2)}$ as

$$L^{(2)} = \frac{1}{\Lambda_0(|\sigma(\tau)|^2 - 1)} \begin{pmatrix} l_{xx}^{(2)} & l_{xp}^{(2)} \\ l_{xp}^{(2)} & l_{pp}^{(2)} \end{pmatrix}, \tag{C3}$$

where

$$l_{xx}^{(2)} = \tau + \tau\sigma_{xp}(\tau)^2 - \tau^2\sigma_{xp}(\tau)\sigma_{pp}(\tau) + \tau^3\sigma_{pp}(\tau)^2, \tag{C4}$$

$$l_{xp}^{(2)} = -\tau\sigma_{xx}(\tau)\sigma_{xp}(\tau) + \frac{\tau^2}{2}[\sigma_{xx}(\tau)\sigma_{pp}(\tau) + \sigma_{xp}(\tau)^2 - 1] - \frac{\tau^3}{3}\sigma_{xp}(\tau)\sigma_{pp}(\tau), \tag{C5}$$

$$l_{pp}^{(2)} = \tau\sigma_{xx}(\tau)^2 - \tau^2\sigma_{xx}(\tau)\sigma_{xp}(\tau) + \frac{\tau^3}{3}[1 + \sigma_{xp}(\tau)^2]. \tag{C6}$$

Then $L^{(2)}$ has eigenvalues

$$\alpha \pm \sqrt{\alpha^2 - \tau^2\left[\sigma_{xx}(\tau) - \tau\sigma_{xp}(\tau) + \frac{\tau^2}{3}\sigma_{pp}(\tau)\right]^2 - \frac{\tau^4}{12}(|\sigma(\tau)| - 1)^2}, \tag{C7}$$

with

$$\alpha(\tau) = \frac{\tau}{2}\left\{1 + \sigma_{xx}(\tau)^2 - \sigma_{xp}(\tau)[\sigma_{xx}(\tau) + \sigma_{pp}(\tau)]\tau + \frac{\tau^2}{3}[1 + \sigma_{pp}(\tau)^2] + \sigma_{xp}(\tau)^2\left(1 + \frac{\tau^2}{3}\right)\right\}. \tag{C8}$$

In order for phonon-number-resolving detection to become optimal we then seek the symplectic transformation which gives the Williamson normal form of $L^{(2)}$. For a single-mode system this can be recognized by first diagonalizing $L^{(2)}$ with a phase shift $\left(\begin{smallmatrix} \cos\psi & \sin\psi \\ -\sin\psi & \cos\psi \end{smallmatrix}\right)$, followed by a squeezing $\mathrm{diag}(e^z, e^{-z})$. The phase shift diagonalizes $L^{(2)}$, which has eigenvalues D_1 and D_2. The symplectic eigenvalue of $L^{(2)}$ is then $\sqrt{D_1 D_2}$, and so the squeezing z required to bring $L^{(2)}$ into its normal form is $e^{2z} = e^{\frac{1}{2}|\ln D_1 - \ln D_2|}$.

Thus the required squeezing is

$$e^{2z} = \sqrt{\frac{1 + \sqrt{1 - \frac{1}{\alpha^2}\left\{\tau^2\left[\sigma_{xx}(\tau) - \tau\sigma_{xp}(\tau) + \frac{\tau^2}{3}\sigma_{pp}(\tau)\right]^2 + \frac{\tau^4}{12}[|\sigma(\tau)| - 1]^2\right\}}}{1 - \sqrt{1 - \frac{1}{\alpha^2}\left\{\tau^2\left[\sigma_{xx}(\tau) - \tau\sigma_{xp}(\tau) + \frac{\tau^2}{3}\sigma_{pp}(\tau)\right]^2 + \frac{\tau^4}{12}[|\sigma(\tau)| - 1]^2\right\}}}}. \tag{C9}$$

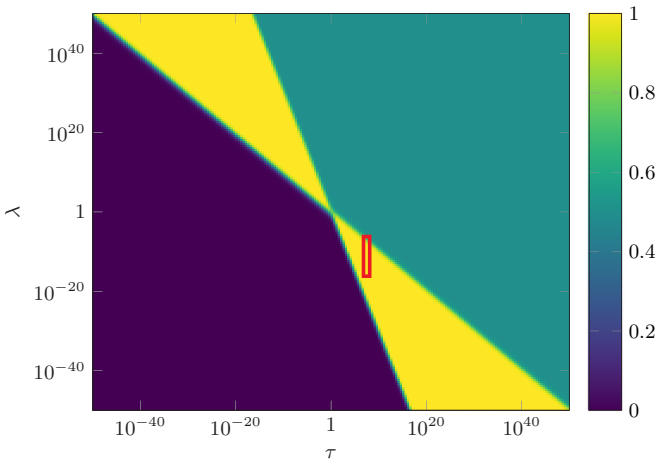

FIG. 4. Ratio of quantum Fisher information against classical Fisher information for optimal homodyne quadrature $[F(\Lambda;\theta_{\mathrm{opt}})/H(\Lambda)]$, plotted for $\kappa_{\mathrm{th}} = 1$ and $r = 0$. The red rectangle is representative of the MAQRO parameter regime.

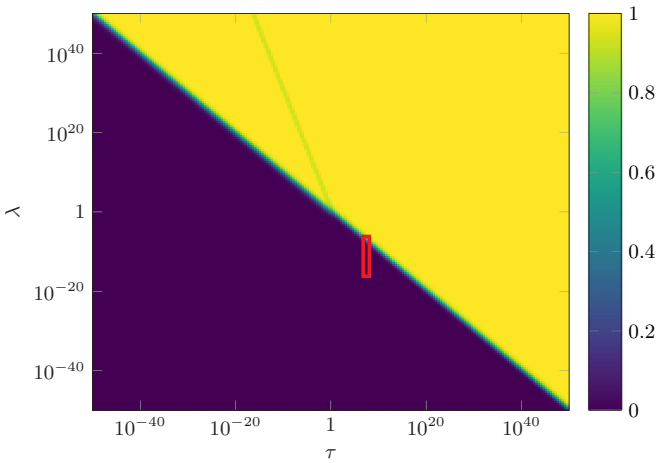

FIG. 5. Ratio of quantum Fisher information against classical Fisher information for heterodyne detection $[F(\Lambda)/H(\Lambda)]$, plotted for $\kappa_{\mathrm{th}} = 1$ and $r = 0$. The red rectangle is representative of the MAQRO parameter regime.

APPENDIX D: OPTIMALITY OF DETECTION SCHEMES

Our bounds cover a range of settings with Λ_0^2 prefactoring the bounds and their ratios being a function of only λ, τ, $\kappa_{\rm th}$, and squeezing $re^{i\phi}$ (with parameters such as homodyne angle θ representing different measurement choices rather than properties of the system). This allows comparison of our bounds in terms of these parameters alone, perhaps the simplest case being where we assume trapping allows us to take $\kappa_{\rm th} = 1$ and that no external squeezing is applied.

1. Homodyne

For $\kappa_{\rm th} = 1$ and $r = 0$ we can easily compare the QCRB with the optimal homodyne CRB numerically across the λ and τ variables in Fig. 4. The analytic form of the ratio is

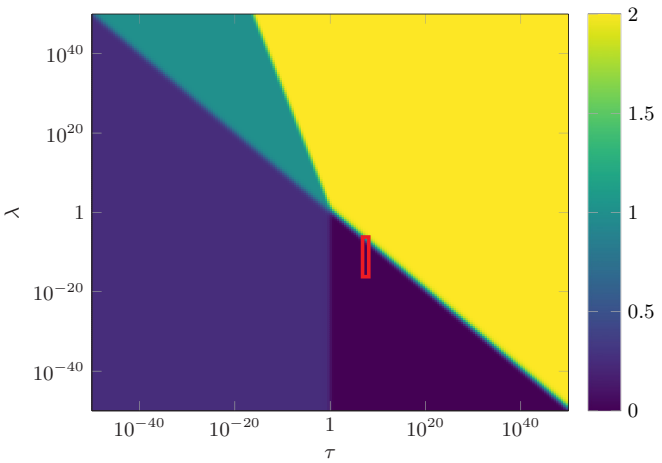

FIG. 6. Ratio of classical Fisher information for heterodyne detection against classical Fisher information for homodyne detection of the optimal quadrature, plotted for $\kappa_{\rm th} = 1$ and $r = 0$. The red rectangle is representative of the MAQRO parameter regime.

$$R = \frac{\tau^4\left\{\left[\lambda\tau\left(1+\frac{\tau^2}{3}+\frac{\tau^3}{12}\lambda\right)+1\right]^2-1\right\}}{72\left(1+\frac{\tau^2}{3}+\frac{\tau^3}{6}\lambda-\frac{\sqrt{9+3\tau^2+\tau^4}}{3}\right)^2\left[\left(1+\frac{\tau^2}{3}+\frac{\tau^3}{12}\lambda\right)^2-\frac{1}{2}\left(1+\frac{\tau^2}{3}\right)\left(1+\frac{\tau^2}{3}+\frac{\tau^3}{6}\lambda\right)\right]}. \tag{D1}$$

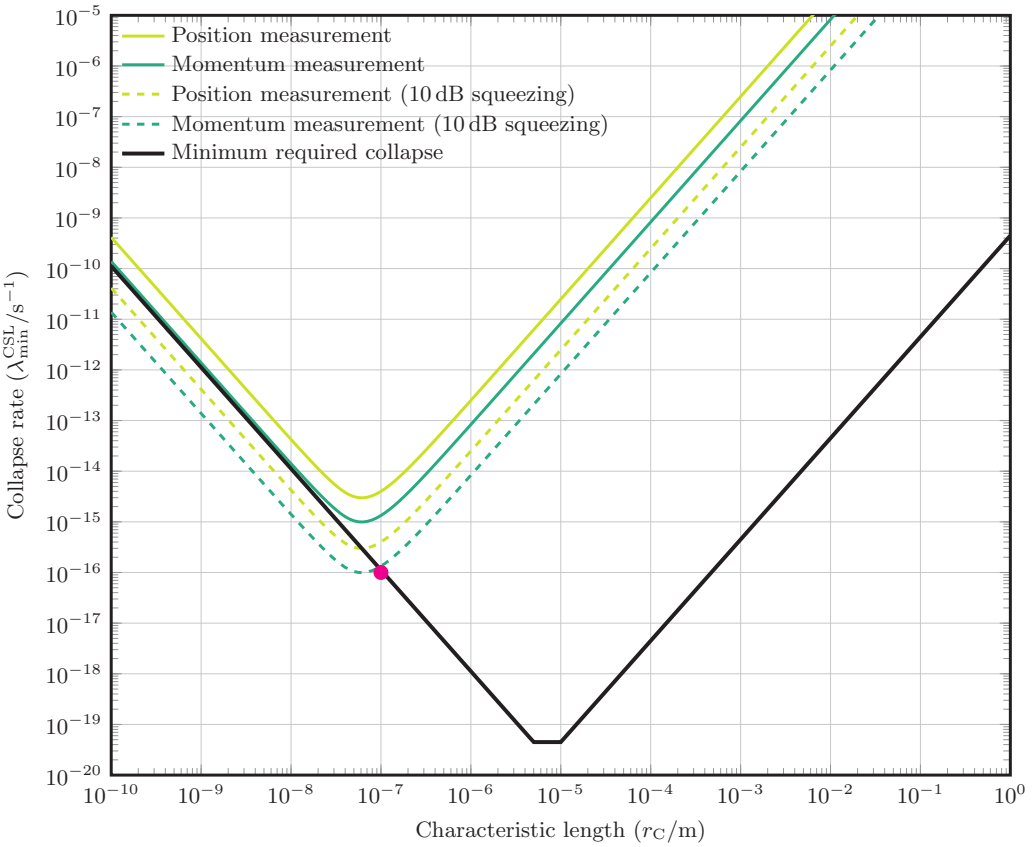

FIG. 7. Bounds plotted for a $r_{\rm s} = 100$ nm sphere of mass 5.5×10^9 u with values otherwise as Table I. The minimum required collapse rate given is based on the criteria of Ref. [7]. The magenta dot represents the values originally proposed by Ghirardi *et al.* [15].

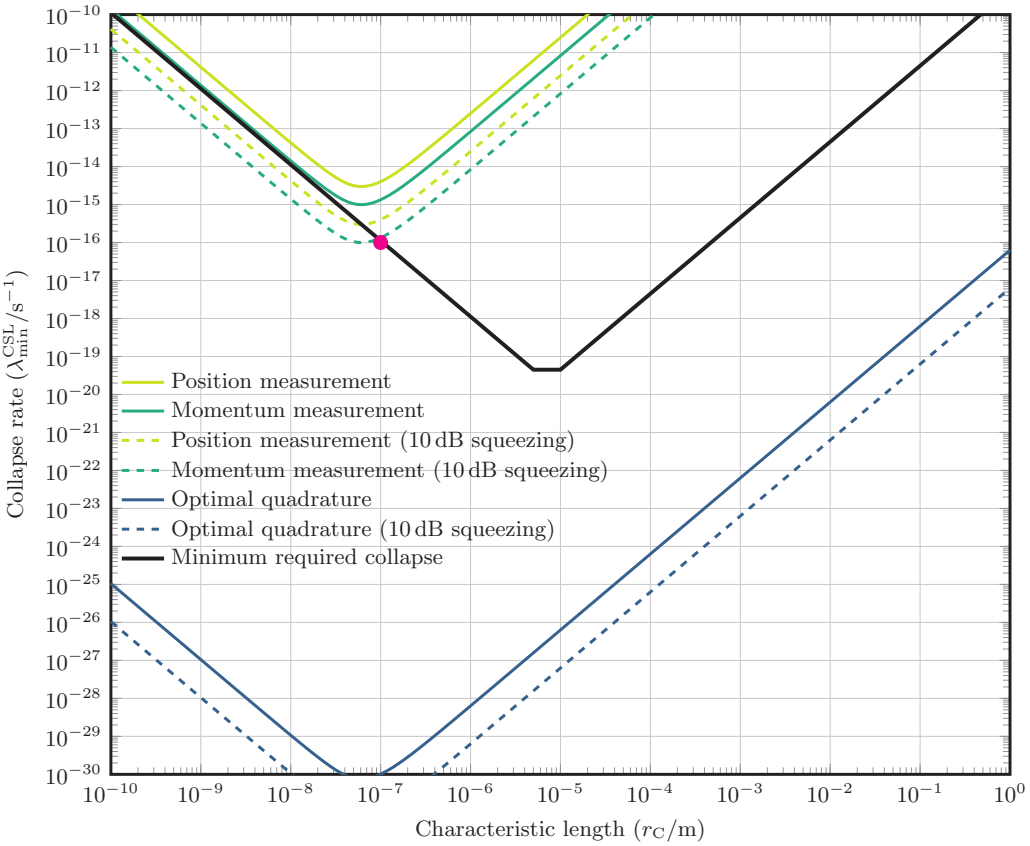

FIG. 8. Bounds plotted for a $r_{\mathrm{s}} = 100$ nm sphere of mass 5.5×10^9 u with values otherwise as Table I. The minimum required collapse rate given is based on the criteria of Ref. [7]. The magenta dot represents the values originally proposed by Ghirardi *et al.* [15].

2. Heterodyne

For $\kappa_{\mathrm{th}} = 1$ and $r = 0$ we can easily compare the QCRB with the heterodyne CRB numerically across the λ and τ variables in Fig. 5. The analytic form of the ratio is

$$R = \frac{\left\{\left[\lambda\tau\left(1+\frac{\tau^2}{3}+\lambda\frac{\tau^3}{12}\right)+1\right]^2-1\right\}\left[\left(1+\frac{\tau^2}{3}+\lambda\frac{\tau^3}{12}\right)^2+\left(1+\frac{\tau^2}{6}\right)^2\right]}{16\left(1+\frac{\tau}{2}\lambda\right)^2\left(1+\frac{\tau^2}{4}+\frac{\lambda\tau^3}{24}\right)^2\left[\left(1+\frac{\tau^2}{3}+\frac{\lambda\tau^3}{12}\right)^2-\frac{1}{2}\left(1+\frac{\tau^2}{3}\right)\left(1+\frac{\tau^2}{3}+\frac{\lambda\tau^3}{6}\right)\right]}. \tag{D2}$$

3. Homodyne and heterodyne

In the same $\kappa_{\mathrm{th}} = 1$ and $r = 0$ case we can compare the optimal homodyne CRB against the heterodyne CRB numerically across the λ and τ variables in Fig. 6. This demonstrates no more than a factor of two advantage for heterodyne in the $\tau \gg 1$ and $\lambda \gg 1$, while in the $\lambda \ll 1$ regime the homodyne has a near unbounded advantage.

The analytic form of the ratio [which can be seen from Eqs. (D1) and (D2)] is

$$R = \frac{9\left[\left(1+\frac{\tau^2}{3}+\lambda\frac{\tau^3}{12}\right)^2+\left(1+\frac{\tau^2}{6}\right)^2\right]\left(1+\frac{\tau^2}{3}+\frac{\tau^3}{6}\lambda-\frac{\sqrt{9+3\tau^2+\tau^4}}{3}\right)^2}{2\tau^4\left(1+\frac{\tau}{2}\lambda\right)^2\left(1+\frac{\tau^2}{4}+\frac{\lambda\tau^3}{24}\right)^2}. \tag{D3}$$

APPENDIX E: TESTS OF CONTINUOUS SPONTANEOUS LOCALIZATION

For MAQRO the minimum resolvable λ^{CSL} for position and momentum can be seen in Fig. 7, plotted for a $r_{\mathrm{s}} = 100$ nm sphere of mass 5.5×10^9 u with values otherwise as Table I, where the black line is based on the minimum required CSL strength proposed in Toroš *et al.* [7]. This plot shows the potential improvements; with MAQRO already competitive in 10^{-8}–10^{-5} m, squeezing allows a test down to the lower bound for $r_{\mathrm{C}} < 10^{-7}$ m and significant improvement on reported results up to $r_{\mathrm{C}} = 10^{-5}$ m.

This is plotted in Fig. 8, plotted again for a $r_{\mathrm{s}} = 100$ nm sphere of mass 5.5×10^9 u with values otherwise as Table I. As might be guessed from the significant gap in Fig. 2 the optimal quadrature allows for a categorical test of CSL. This bound can be reduced through squeezing, and the fundamental

limit given by the QCRB will further allow a superior precision through a saturating measurement. Such improvements, however, offer little significance, as the QCRB will give a lower bound no less than that of the optimal quadrature.

[1] A. Bassi and G. Ghirardi, Dynamical reduction models, Phys. Rep. **379**, 257 (2003).

[2] A. Bassi, K. Lochan, S. Satin, T. P. Singh, and H. Ulbricht, Models of wave-function collapse, underlying theories, and experimental tests, Rev. Mod. Phys. **85**, 471 (2013).

[3] A. Bassi, D. Dürr, and G. Hinrichs, Uniqueness of the Equation for Quantum State Vector Collapse, Phys. Rev. Lett. **111**, 210401 (2013).

[4] A. Bassi, A. Großardt, and H. Ulbricht, Gravitational decoherence, Classical Quant. Grav. **34**, 193002 (2017).

[5] P. Pearle, Combining stochastic dynamical state-vector reduction with spontaneous localization, Phys. Rev. A **39**, 2277 (1989).

[6] G. C. Ghirardi, P. Pearle, and A. Rimini, Markov processes in Hilbert space and continuous spontaneous localization of systems of identical particles, Phys. Rev. A **42**, 78 (1990).

[7] M. Toroš, G. Gasbarri, and A. Bassi, Colored and dissipative continuous spontaneous localization model and bounds from matter-wave interferometry, Phys. Lett. A **381**, 3921 (2017).

[8] F. Karolyhazy, Gravitation and quantum mechanics of macroscopic objects, Nuovo Cimento A (1965–1970) **42**, 390 (1966).

[9] L. Diósi, A universal master equation for the gravitational violation of quantum mechanics, Phys. Lett. A **120**, 377 (1987).

[10] L. Diósi, Models for universal reduction of macroscopic quantum fluctuations, Phys. Rev. A **40**, 1165 (1989).

[11] R. Penrose, On gravity's role in quantum state reduction, Gen. Relativ. Grav. **28**, 581 (1996).

[12] M. Bahrami, A. Smirne, and A. Bassi, Role of gravity in the collapse of a wave function: A probe into the Diósi-Penrose model, Phys. Rev. A **90**, 062105 (2014).

[13] J. Ellis, S. Mohanty, and D. V. Nanopoulos, Quantum gravity and the collapse of the wavefunction, Phys. Lett. B **221**, 113 (1989).

[14] M. R. Gallis and G. N. Fleming, Environmental and spontaneous localization, Phys. Rev. A **42**, 38 (1990).

[15] G. C. Ghirardi, A. Rimini, and T. Weber, Unified dynamics for microscopic and macroscopic systems, Phys. Rev. D **34**, 470 (1986).

[16] M. Carlesso, A. Bassi, P. Falferi, and A. Vinante, Experimental bounds on collapse models from gravitational wave detectors, Phys. Rev. D **94**, 124036 (2016).

[17] B. Helou, B. J. J. Slagmolen, D. E. McClelland, and Y. Chen, LISA pathfinder appreciably constrains collapse models, Phys. Rev. D **95**, 084054 (2017).

[18] M. Carlesso, M. Paternostro, H. Ulbricht, A. Vinante, and A. Bassi, Non-interferometric test of the continuous spontaneous localization model based on rotational optomechanics, New J. Phys. **20**, 083022 (2018).

[19] A. Vinante, R. Mezzena, P. Falferi, M. Carlesso, and A. Bassi, Improved Noninterferometric Test of Collapse Models Using Ultracold Cantilevers, Phys. Rev. Lett. **119**, 110401 (2017).

[20] Y. Li, A. M. Steane, D. Bedingham, and G. A. D. Briggs, Detecting continuous spontaneous localization with charged bodies in a Paul trap, Phys. Rev. A **95**, 032112 (2017).

[21] O. Romero-Isart, A. C. Pflanzer, F. Blaser, R. Kaltenbaek, N. Kiesel, M. Aspelmeyer, and J. I. Cirac, Large Quantum Superpositions and Interference of Massive Nanometer-Sized Objects, Phys. Rev. Lett. **107**, 020405 (2011).

[22] O. Romero-Isart, Quantum superposition of massive objects and collapse models, Phys. Rev. A **84**, 052121 (2011).

[23] M. Scala, M. S. Kim, G. W. Morley, P. F. Barker, and S. Bose, Matter-Wave Interferometry of a Levitated Thermal Nano-Oscillator Induced and Probed by a Spin, Phys. Rev. Lett. **111**, 180403 (2013).

[24] C. Wan, M. Scala, G. W. Morley, ATM. A. Rahman, H. Ulbricht, J. Bateman, P. F. Barker, S. Bose, and M. S. Kim, Free Nano-Object Ramsey Interferometry for Large Quantum Superpositions, Phys. Rev. Lett. **117**, 143003 (2016).

[25] S. Bose, A. Mazumdar, G. W. Morley, H. Ulbricht, M. Toroš, M. Paternostro, A. A. Geraci, P. F. Barker, M. S. Kim, and G. Milburn, Spin Entanglement Witness for Quantum Gravity, Phys. Rev. Lett. **119**, 240401 (2017).

[26] M. J. Weaver, D. Newsom, F. Luna, W. Löffler, and D. Bouwmeester, Phonon interferometry for measuring quantum decoherence, Phys. Rev. A **97**, 063832 (2018).

[27] R. Kaltenbaek, G. Hechenblaikner, N. Kiesel, O. Romero-Isart, K. C. Schwab, U. Johann, and M. Aspelmeyer, Macroscopic quantum resonators (MAQRO), Exp. Astron. **34**, 123 (2012).

[28] R. Kaltenbaek, M. Aspelmeyer, P. F. Barker, A. Bassi, J. Bateman, K. Bongs, S. Bose, C. Braxmaier, Č. Brukner, B. Christophe, M. Chwalla, P.-F. Cohadon, A. M. Cruise, C. Curceanu, K. Dholakia, L. Diósi, K. Döringshoff, W. Ertmer, J. Gieseler, N. Gürlebeck, G. Hechenblaikner, A. Heidmann, S. Herrmann, S. Hossenfelder, U. Johann, N. Kiesel, M. Kim, C. Lämmerzahl, A. Lambrecht, M. Mazilu, G. J. Milburn, H. Müller, L. Novotny, M. Paternostro, A. Peters, I. Pikovski, A. Pilan-Zanoni, E. M. Rasel, S. Reynaud, C. J. Riedel, M. Rodrigues, L. Rondin, A. Roura, W. P. Schleich, J. Schmiedmayer, T. Schuldt, K. C. Schwab, M. Tajmar, G. M. Tino, H. Ulbricht, R. Ursin, and V. Vedral, Macroscopic quantum resonators (MAQRO): 2015 update, EPJ Quant. Tech. **3**, 5 (2016).

[29] European Space Agency, CDF study report: QPPF—Assessment of a quantum physics payload platform, Tech. Rep. CDF-183(C), European Space Agency (2018).

[30] G. Tóth and I. Apellaniz, Quantum metrology from a quantum information science perspective, J. Phys. A **47**, 424006 (2014).

[31] R. Demkowicz-Dobrzański, M. Jarzyna, and J. Kołodyński, Quantum limits in optical interferometry, in *Progress in Optics*, Vol. 60, edited by E. Wolf (Elsevier, Amsterdam, 2015), pp. 345–435.

[32] C. M. Caves, Quantum-mechanical noise in an interferometer, Phys. Rev. D **23**, 1693 (1981).

[33] The LIGO Scientific Collaboration, A gravitational wave observatory operating beyond the quantum shot-noise limit, Nat. Phys. **7**, 962 (2011).

[34] H. Grote, K. Danzmann, K. L. Dooley, R. Schnabel, J. Slutsky, and H. Vahlbruch, First Long-Term Application of Squeezed States of Light in a Gravitational-Wave Observatory, Phys. Rev. Lett. **110**, 181101 (2013).

[35] The LIGO Scientific Collaboration, Enhanced sensitivity of the LIGO gravitational wave detector by using squeezed states of light, Nat. Photonics **7**, 613 (2013).

[36] H. Vahlbruch, M. Mehmet, K. Danzmann, and R. Schnabel, Detection of 15 dB Squeezed States of Light and Their Application for the Absolute Calibration of Photoelectric Quantum Efficiency, Phys. Rev. Lett. **117**, 110801 (2016).

[37] M. A. Taylor, J. Knittel, and W. P. Bowen, Fundamental constraints on particle tracking with optical tweezers, New J. Phys. **15**, 023018 (2013).

[38] M. A. Taylor, J. Janousek, V. Daria, J. Knittel, B. Hage, H.-A. Bachor, and W. P. Bowen, Subdiffraction-Limited Quantum Imaging within a Living Cell, Phys. Rev. X **4**, 011017 (2014).

[39] M. Malnou, D. A. Palken, B. M. Brubaker, L. R. Vale, G. C. Hilton, and K. W. Lehnert, Squeezed Vacuum Used to Accelerate the Search for a Weak Classical Signal, Phys. Rev. X **9**, 021023 (2019).

[40] A. Pontin, M. Bonaldi, A. Borrielli, F. S. Cataliotti, F. Marino, G. A. Prodi, E. Serra, and F. Marin, Squeezing a Thermal Mechanical Oscillator by Stabilized Parametric Effect on the Optical Spring, Phys. Rev. Lett. **112**, 023601 (2014).

[41] M. Rashid, T. Tufarelli, J. Bateman, J. Vovrosh, D. Hempston, M. S. Kim, and H. Ulbricht, Experimental Realization of a Thermal Squeezed State of Levitated Optomechanics, Phys. Rev. Lett. **117**, 273601 (2016).

[42] C. J. Riedel, Direct detection of classically undetectable dark matter through quantum decoherence, Phys. Rev. D **88**, 116005 (2013).

[43] C. J. Riedel, Decoherence from classically undetectable sources: Standard quantum limit for diffusion, Phys. Rev. A **92**, 010101(R) (2015).

[44] C. J. Riedel and I. Yavin, Decoherence as a way to measure extremely soft collisions with dark matter, Phys. Rev. D **96**, 023007 (2017).

[45] B. Collett and P. Pearle, Wavefunction collapse and random walk, Found. Phys. **33**, 1495 (2003).

[46] L. Diósi, Testing Spontaneous Wave-Function Collapse Models on Classical Mechanical Oscillators, Phys. Rev. Lett. **114**, 050403 (2015).

[47] L. P. Ghislain and W. W. Webb, Scanning-force microscope based on an optical trap, Opt. Lett. **18**, 1678 (1993).

[48] A. Pralle, E.-L. Florin, E. Stelzer, and J. Hörber, Local viscosity probed by photonic force microscopy, Appl. Phys. A **66**, S71 (1998).

[49] M. G. Genoni, O. S. Duarte, and A. Serafini, Unravelling the noise: The discrimination of wave function collapse models under time-continuous measurements, New J. Phys. **18**, 103040 (2016).

[50] S. McMillen, M. Brunelli, M. Carlesso, A. Bassi, H. Ulbricht, M. G. A. Paris, and M. Paternostro, Quantum-limited estimation of continuous spontaneous localization, Phys. Rev. A **95**, 012132 (2017).

[51] A. Monras and M. G. A. Paris, Optimal Quantum Estimation of Loss in Bosonic Channels, Phys. Rev. Lett. **98**, 160401 (2007).

[52] G. Adesso, F. Dell'Anno, S. De Siena, F. Illuminati, and L. A. M. Souza, Optimal estimation of losses at the ultimate quantum limit with non-Gaussian states, Phys. Rev. A **79**, 040305(R) (2009).

[53] S. I. Knysh and G. A. Durkin, Estimation of phase and diffusion: Combining quantum statistics and classical noise, arXiv:1307.0470.

[54] M. D. Vidrighin, G. Donati, M. G. Genoni, X.-M. Jin, W. S. Kolthammer, M. S. Kim, A. Datta, M. Barbieri, and I. A. Walmsley, Joint estimation of phase and phase diffusion for quantum metrology, Nat. Commun. **5**, 3532 (2014).

[55] M. Tsang, Quantum limit to subdiffraction incoherent optical imaging, Phys. Rev. A **99**, 012305 (2019).

[56] S. Ng, S. Z. Ang, T. A. Wheatley, H. Yonezawa, A. Furusawa, E. H. Huntington, and M. Tsang, Spectrum analysis with quantum dynamical systems, Phys. Rev. A **93**, 042121 (2016).

[57] A. Ferraro, S. Olivares, and M. G. A. Paris, Gaussian states in continuous variable quantum information (Bibliopolis, Napoli, 2005), arXiv:quant-ph/0503237.

[58] D. Windey, C. Gonzalez-Ballestero, P. Maurer, L. Novotny, O. Romero-Isart, and R. Reimann, Cavity-Based 3D Cooling of a Levitated Nanoparticle Via Coherent Scattering, Phys. Rev. Lett. **122**, 123601 (2019).

[59] U. Delić, M. Reisenbauer, D. Grass, N. Kiesel, V. Vuletić, and M. Aspelmeyer, Cavity Cooling of a Levitated Nanosphere by Coherent Scattering, Phys. Rev. Lett. **122**, 123602 (2019).

[60] O. Romero-Isart, L. Clemente, C. Navau, A. Sanchez, and J. I. Cirac, Quantum Magnetomechanics with Levitating Superconducting Microspheres, Phys. Rev. Lett. **109**, 147205 (2012).

[61] C. Gonzalez-Ballestero, P. Maurer, D. Windey, L. Novotny, R. Reimann, and O. Romero-Isart, Theory for cavity cooling of levitated nanoparticles via coherent scattering: Master equation approach, Phys. Rev. A **100**, 013805 (2019).

[62] H. J. Carmichael, *Statistical Methods in Quantum Optics 1: Master Equations and Fokker-Planck Equations*, Theoretical and Mathematical Physics (Springer-Verlag, Berlin, 1999).

[63] F. Nicacio, R. N. P. Maia, F. Toscano, and R. O. Vallejos, Phase space structure of generalized Gaussian cat states, Phys. Lett. A **374**, 4385 (2010).

[64] A. Serafini, *Quantum Continuous Variables: A Primer of Theoretical Methods* (CRC Press, Boca Raton, 2017).

[65] S. M. Barnett and P. M. Radmore, *Methods in Theoretical Quantum Optics* (Oxford University Press, Oxford, 2002).

[66] S. M. Kay, *Fundamentals of Statistical Signal Processing: Estimation Theory* (Prentice-Hall PTR, New York, 1998).

[67] C. W. Helstrom, *Quantum Detection and Estimation Theory* (Academic Press, New York, 1976).

[68] A. Holevo, *Probabilistic and Statistical Aspects of Quantum Theory* (Edizioni della Normale, Pisa, 2011).

[69] M. G. A. Paris, Quantum estimation for quantum technology, Int. J. Quant. Inform. **7**, 125 (2009).

[70] A. Monras, Phase space formalism for quantum estimation of Gaussian states, arXiv:1303.3682.

[71] D. Šafránek, A. R. Lee, and I. Fuentes, Quantum parameter estimation using multi-mode Gaussian states, New J. Phys. **17**, 073016 (2015).

[72] G. Adesso, S. Ragy, and A. R. Lee, Continuous variable quantum information: Gaussian states and beyond, Open Syst. Inf. Dyn. **21**, 1440001 (2014).

[73] J. Shapiro and S. Wagner, Phase and amplitude uncertainties in heterodyne detection, IEEE J. Quantum Electron. **20**, 803 (1984).

[74] U. Leonhardt and H. Paul, Measuring the quantum state of light, Prog. Quantum Electron. **19**, 89 (1995).

[75] S. L. Braunstein and C. M. Caves, Statistical Distance and the Geometry of Quantum States, Phys. Rev. Lett. **72**, 3439 (1994).

[76] J. D. Cohen, S. M. Meenehan, G. S. MacCabe, S. Gröblacher, A. H. Safavi-Naeini, F. Marsili, M. D. Shaw, and O. Painter, Phonon counting and intensity interferometry of a nanomechanical resonator, Nature (London) **520**, 522 (2015).

[77] S. Hong, R. Riedinger, I. Marinković, A. Wallucks, S. G. Hofer, R. A. Norte, M. Aspelmeyer, and S. Gröblacher, Hanbury Brown and Twiss interferometry of single phonons from an optomechanical resonator, Science **358**, 203 (2017).

[78] K. Piscicchia, A. Bassi, C. Curceanu, R. D. Grande, S. Donadi, B. C. Hiesmayr, and A. Pichler, CSL collapse model mapped with the spontaneous radiation, Entropy **19**, 319 (2017).